Supplementary Materials

Alkalinity-controlled zeolite nucleation and growth: ultrafast synthesis of total-morphology zeolite L mesocrystals and adsorption evaluation

1. The synthesis of total-morphology zeolite L mesocrystals

Supplementary Table 1. The synthesis conditions, additional requirements, and the corresponding product morphology and size of zeolite L in previous literature and in this work

Products morphology	**Starting gel composition K_2O:Al_2O_3:SiO_2:H_2O**	**Additional requirements & modifiers**	**Heating condition**		**Particle size (*d* × *l*, nm)**	**Refs.**
			T [a] **(h)**	***T*** **(°C)**		
nanoclusters	0.5:0.05:1:20	-	4	175	60 × 80, domain ~15	[1]
nanoclusters	0.462:0.0495:1:20.44	-	6	170	80 × 100, domain ~30	[2]
nanoclusters	0.5:0.05:1:20	-	4	170	200 × 400, domain ~15	[3]
nanoclusters	**0.575:0.1333:1:20**	**-**	**4 (1)**	**190**	**(30-40) × (60-80), domain (10-15) × (15-20)**	**This work**
nanoclusters	**0.675:0.1333:1:20**	**-**	**1**	**190**	**(60-70) × (100-120), domain (8-12) × (15-20)**	**This work**
nanocrystals	0.280:0.049:1:100.98 (with 88% extra K^+)	silica source is K_2SiO_3	4	180	11 × 32	[4]

nanocrystals (with some nanoclusters)	**0.475:0.1333:1:20**	**-**	**2**	**190**	**15 × (30-35)**	**This work**
disc-like	(0.18 K_2O & 0.183 Na_2O):0.0333:1:13.869	KOH is partially replaced by NaOH	48	160	(1000-1500) × (200-300)	[5]
disc-like	0.51:0.05:1:51.5	1,2,6-hexanetriol (17 wt%)	168	100	1000 × (55-100)	[6]
disc-like	0.51:0.05:1:47.5	C_2H_5OH (4:1 SiO_2)	72	150	(2000-3000) × (150-200)	[7]
disc-like	0.34:0.103:1:16.6	triethanol amine (0.133:1 SiO_2)	144	120	1500 × 300	[8]
disc-like	**0.375:0.1333:1:20**	**-**	**10 (2)**	**190**	**300 × 100**	**This work**
disc-like (fragmented)	**0.425:0.1333:1:20**	**-**	**2**	**190**	**200 × (50-60)**	**This work**
cylindrical	0.3:0.09:1:16	-	20	160	1500 × 1500	[3]
cylindrical	0.25:0.08:1:15	-	72	170	(2000-2500) × (2000-2500)	[9]
cylindrical	0.51:0.025:1:51.5	-	24	180	1000 × 1500	[10]
cylindrical	**0.325:0.1333:1:20**	**-**	**18**	**190**	**(1500-2000) × (1500-2000)**	**This work**

[a]The time annotated in parentheses is the shortest hydrothermal time required to obtain the products with high crystallinity under the corresponding condition, based on the subsequent tracking of the crystallization process.

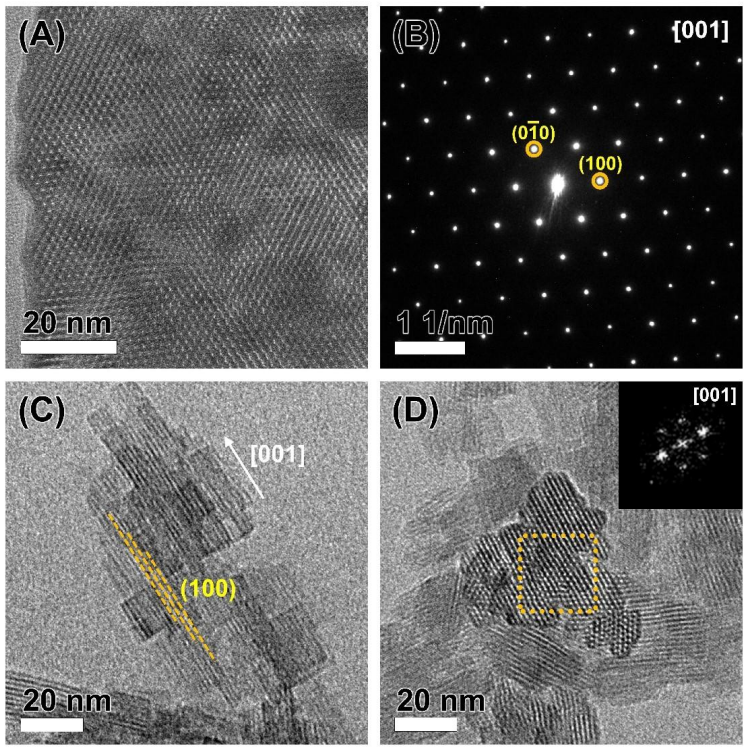

Supplementary Figure 1. (A) The HR-TEM image of LTL-LB and (B) the corresponding SAED result. (C) and (D) is the HR-TEM images of LTL-HB captured perpendicular/along the [001] direction. Inset of (D): the fast Fourier transform (FFT) analysis result of the selected area.

Supplementary Table 2. The texture properties and elemental composition information of different zeolite L samples

Samples	S_{BET} (m^2/g)	S_{micro} [a] (m^2/g)	V_{micro} [a] (cm^3/g)	S_{ext} [a] (m^2/g)	V_{meso} [b] (cm^3/g)	SAR [c]
LTL-0.65	386	377	0.142	9	0.012	2.60
LTL-0.75 (LB)	388	368	0.140	20	0.156	2.55
LTL-0.85	413	332	0.132	81	0.384	2.48
LTL-0.95	432	320	0.129	112	0.516	2.40

LTL-1.15 (HB)	457	238	0.099	219	0.710	2.32
LTL-1.35	464	218	0.093	246	0.775	2.29

[a]by t-plot method. [b]using BJH method by the desorption data (pore width: ~2.0-50 nm). [c]by the ICP-AES analysis.

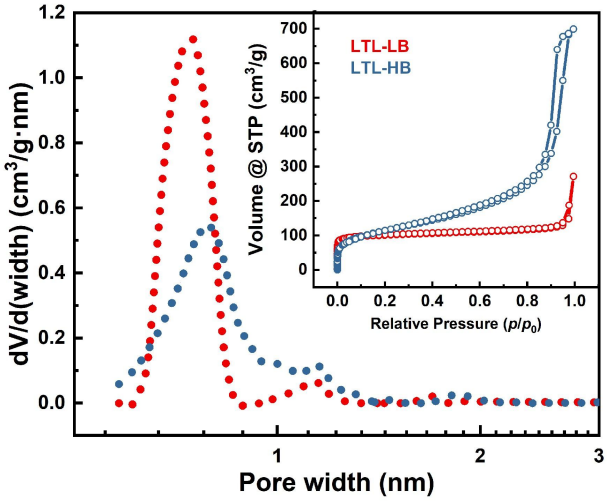

Supplementary Figure 2. The Ar-sorption isotherms of LTL-LB and LTL-HB, and the NLDFT micropore size distribution curves based on the Ar-sorption data.

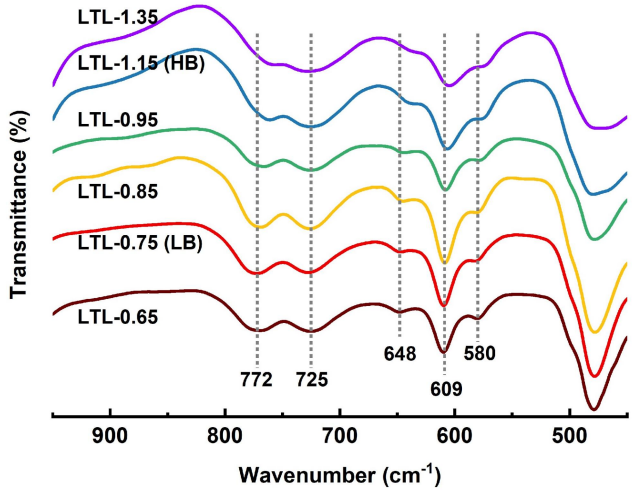

Supplementary Figure 3. The FT-IR spectra of zeolite L synthesized under different alkalinity.

2. Tracking the crystallization processes of LTL-LB and LTL-HB systems

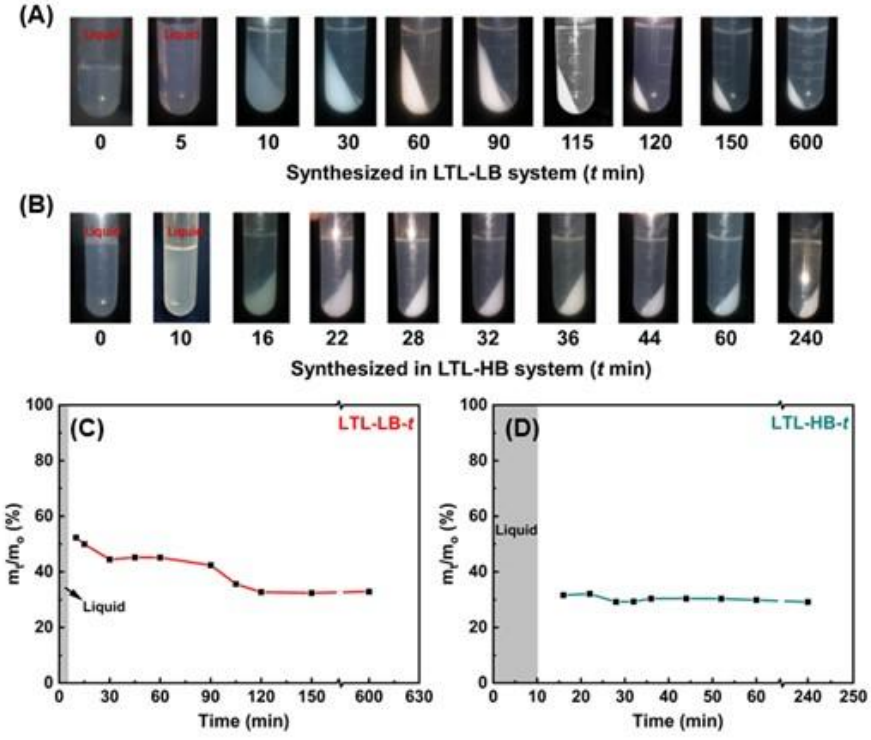

Supplementary Figure 4. Optical photographs of time-resolved intermediates after centrifugation (15000 rpm for 40 min with a relative centrifugal force of 19118 × *g*): A: LTL-LB system; B: LTL-HB system. And C and D show the solid-phase yields of time-resolved intermediates after centrifugation in LTL-LB and LTL-HB systems, respectively.

Annotation for Supplementary Figure 4:

Every intermediate sample (i.e., LTL-LB/HB-*t*) after three times centrifugation were freeze-dried to minimize their structure changes in vacuum at -50 ℃, then the solid-phase yield of each intermediate samples can be obtained by the following equation:

$$\text{The solid-phase yield}=\frac{m_t}{m_0}\times 100\% \quad \text{(S0)}$$

where m_t is the weight of freeze-dried solid powder of intermediate (t: the hydrothermal treatment time in min). And m_0 is the corresponding weight of SiO_2 and Al_2O_3 in feed.

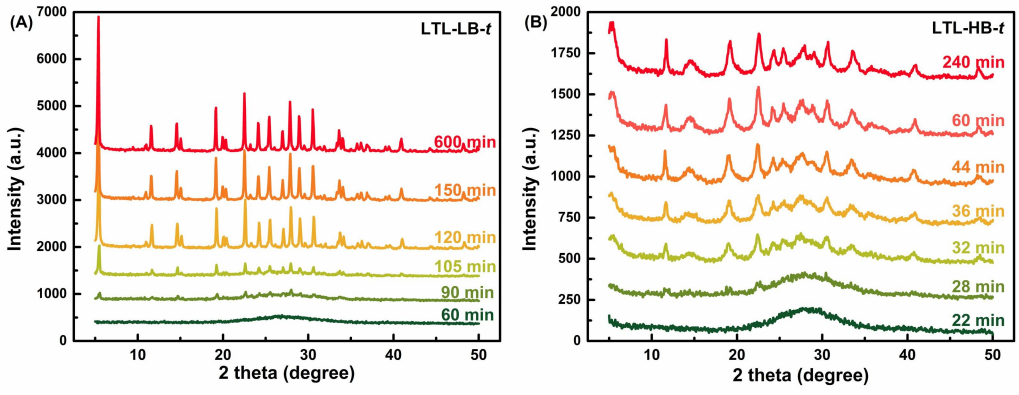

Supplementary Figure 5. XRD patterns of LTL-LB-*t* and LTL-HB-*t* with different hydrothermal treatment times.

Annotation for Supplementary Figure 5 and Figure 3A,B:

The XRD relative crystallinity (RC) of each intermediate samples (i.e., LTL-LB/HB-*t*) in **Figure 3A,B** is defined as:

$$\mathrm{RC} = \frac{A_{XRD}(t)}{A_{XRD}(f)} \cdot 100\% , \qquad \text{(S1)}$$

where $A_{\mathrm{XRD}}(t)$ is the XRD characteristic peak area of the intermediate solid powder (*t*: the hydrothermal treatment time in min). And $A_{\mathrm{XRD}}(f)$ is the XRD characteristic peak area of the final product synthesized under corresponding conditions. The characteristic diffraction peaks in the range of 10-35° are selected for the peak area integration.

Supplementary Table 3. The Si and Al composition change trends in the supernatant and solid phase of the crystallization intermediates

Samples	In the liquid phase			In the solid phase
	[Si]^a (mol/L)	[Al]^a (mmol/L)	SAR_{liquid} ^{a}	SAR_{solid} ^{a}
LTL-LB-5	2.48	165	15.0	(liquid only)
LTL-LB-10	1.80	52.2	34.4	5.24
LTL-LB-15	1.68	23.7	70.8	4.62
LTL-LB-30	1.76	7.96	222	3.81
LTL-LB-45	1.73	7.63	227	3.76
LTL-LB-60	1.60	7.04	228	3.82

LTL-LB-90	1.62	8.69	186	3.56
LTL-LB-105	1.73	3.40	510	3.21
LTL-LB-120	1.76	2.37	743	2.79
LTL-LB-150	1.95	2.14	913	2.62
LTL-LB-600	2.02	1.96	1031	2.55
LTL-HB-10	2.45	164	15.0	(liquid only)
LTL-HB-16	2.15	40.7	52.7	2.71
LTL-HB-22	2.03	31.2	65.0	2.61
LTL-HB-28	2.00	27.9	71.6	2.60
LTL-HB-32	1.99	15.1	132	2.42
LTL-HB-36	2.02	11.1	182	2.39
LTL-HB-44	1.99	5.50	361	2.41
LTL-HB-60	1.93	5.16	374	2.33
LTL-HB-240	1.89	4.76	398	2.32

[a]measured by the ICP-AES analysis.

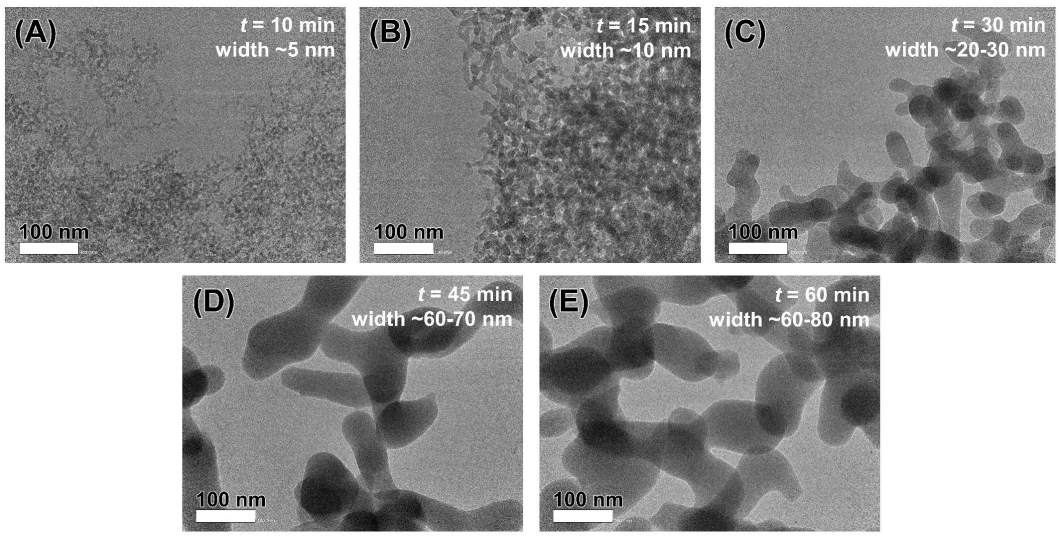

Supplementary Figure 6. The TEM images of LTL-LB-*t* in the induction period, where *t* = (A) 10, (B) 15, (C) 30, (D) 45 and (E) 60 min.

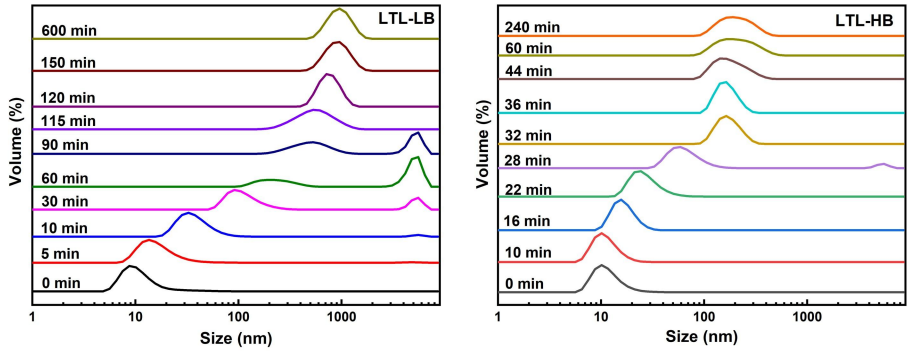

Supplementary Figure 7. Particle size distribution of the evolving precursors during the synthesis crystallization: A) LTL-LB; B) LTL-HB.

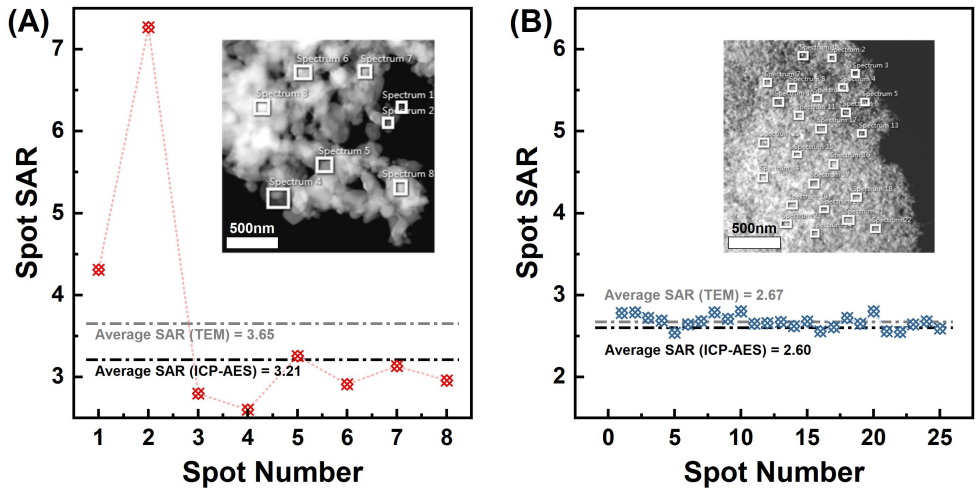

Supplementary Figure 8. The spot EDS results of (A) LTL-LB-105 and (B) LTL-HB-28. Inset: the corresponding HADDF-STEM images marked with the spots for the SAR measurement.

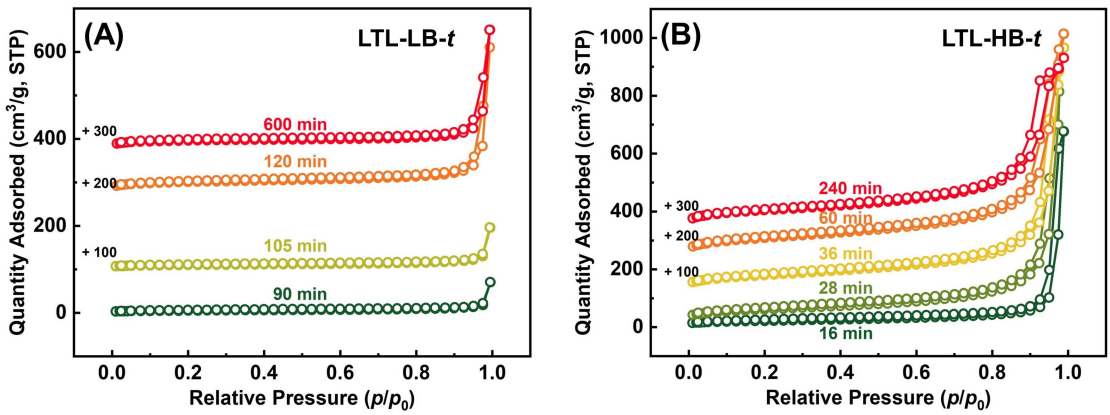

Supplementary Figure 9. N_2-sorption isotherms of the intermediates for (A) LTL-LB-*t* and (B) LTL-HB-*t*.

Supplementary Table 4. The textural properties of LTL-LB-t and LTL-HB-t intermediate samples

Samples	S_{BET} (m^2/g)	S_{micro} [a] (m^2/g)	V_{micro} [a] (cm^3/g)	S_{ext} [a] (m^2/g)	V_{meso} [b] (cm^3/g)	RV [c] (%)	RV/RC
LTL-LB-90	18	7	0.003	11	0.024	2.1	0.18
LTL-LB-105	36	20	0.009	16	0.037	6.4	0.27
LTL-LB-120	402	364	0.140	37	0.186	100	1.03
LTL-LB-600	388	368	0.140	20	0.156	(final product)	
LTL-HB-28	78	24	0.010	54	0.948	10.1	0.71
LTL-HB-32	219	79	0.034	140	1.23	34.3	0.62
LTL-HB-36	285	95	0.041	190	1.16	41.4	0.58
LTL-HB-60	391	174	0.074	217	1.09	74.7	0.77
LTL-HB-240	457	238	0.099	219	0.711	(final product)	

[a]by t-plot method. [b]using BJH method by the desorption data (pore width: ~2.0-50 nm).

[c]the relative V_{micro} (RV) = (V_{micro} of intermediate)/(V_{micro} of the final product) × 100 %.

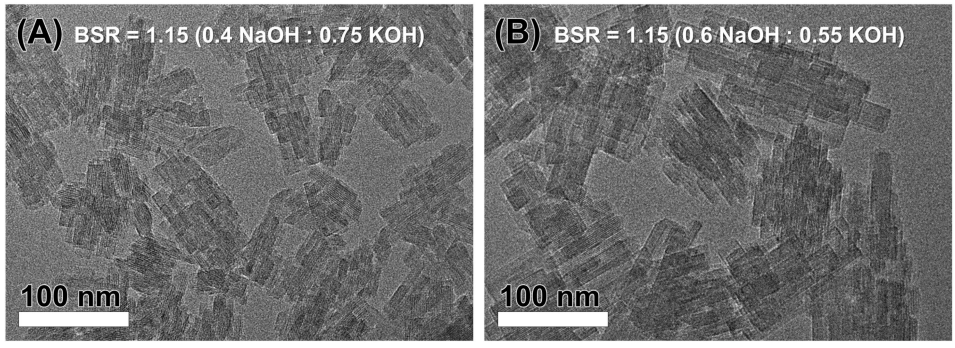

Supplementary Figure 10. TEM of the products obtained by replacing KOH with equimolar NaOH with BSR = 1.15. Where (A) NaOH: KOH = 0.4:0.75, (B) NaOH: KOH = 0.6:0.55.

3. Adsorption performance tests

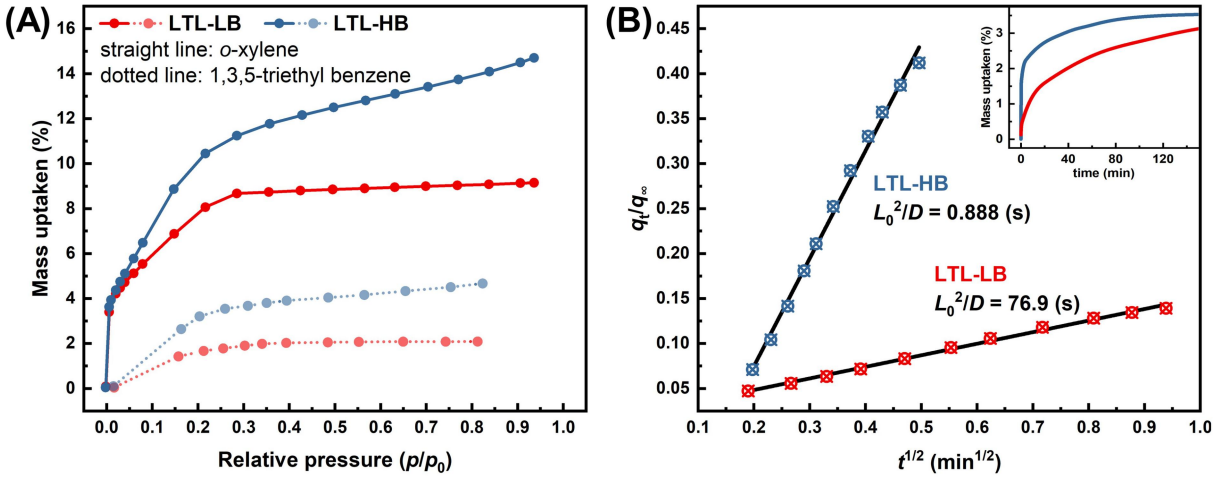

Supplementary Figure 11. (A) The adsorption isotherms of *o*-xylene and 1,3,5-triethyl benzene on LTL-LB and LTL-HB. (B) The characteristic diffusion times of *o*-xylene on different zeolite L, which are calculated by the kinetics uptake profiles (inset) in a short time domain ($p/p_0 = 0 \rightarrow 0.05$).

Note: **Supplementary Figure 11B** is exactly the same as **Figure 9A**, and it is repeated here deliberately for easier viewing and reference.

Annotation for Supplementary Figure 11 and Figure 9A:

The *o*-xylene (kinetic diameter 0.65 nm) and 1,3,5-triethylbenzene (kinetic diameter 0.82 nm) adsorption on zeolite L were measured by IGA. Before the adsorption measurements, 10 mg zeolite sample was degassed for 2 h at 573 K under vacuum with a pressure less than 10^{-3} Pa. After cooling to room temperature, the relative pressure of the corresponding aromatic hydrocarbon gas was controlled by the instrument, the adsorption mass change was measured to the adsorption equilibrium, and the corresponding adsorption kinetic line and thermodynamic adsorption isotherm were obtained.

In particular, for the adsorption process of *o*-xylene at a relative pressure (p/p_0) from 0 to 0.05, it was used to calculate the "characteristic diffusion time (L_0^2/D)"[11]. Where D is the diffusion coefficient of *o*-xylene in the micropore (m^2/s), and L_0 is the intragranular diffusion distance (m). Assuming that the intracrystal diffusion conforms

to the Fick equation, the diffusion of the one-dimensional channel satisfies the following equation:

$$\frac{q_t - q_0}{q_\infty - q_0} = 1 - \frac{2}{\pi^2} \cdot \sum_{n=1}^{\infty} \left[\frac{1}{n^2} \cdot \exp\left(-\frac{n^2 \pi^2 D}{L_0^2} \right) \right], \quad \text{(S2)}$$

in which q_0, q_t and q_∞ are the adsorption amount (mg/mg zeolite) at the initial time, the adsorption time t (s), and the final equilibrium, respectively. For the adsorption process $p/p_0 = 0 \rightarrow 0.05$ ($q_0 = 0$). When the adsorption time is short and far from reaching equilibrium (i.e., the adsorption time $t \rightarrow 0$), the above formula can be simplified as:

$$\frac{q_t}{q_\infty} = \frac{2}{L_0} \cdot \sqrt{\frac{Dt}{\pi}}. \quad \text{(S3)}$$

Therefore, the characteristic diffusion time of o-xylene on different zeolite L mesocrystals can be obtained by the linear fitting of q_t/q_∞ and $t^{1/2}$[11].

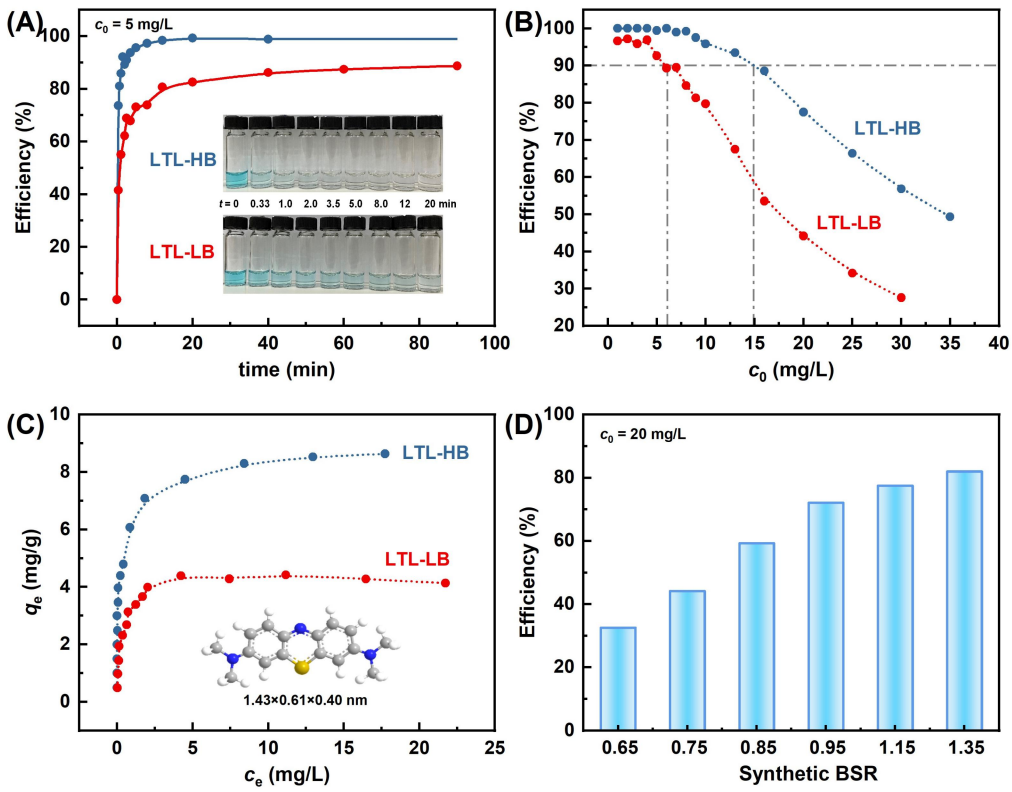

Supplementary Figure 12. (A) The adsorption kinetic curves of methylene blue on LTL-LB/HB (inset: the corresponding optical photos). (B) The equilibrium adsorption efficiency of methylene blue on LTL-LB/HB with different initial concentrations. (C)

The adsorption isotherms of methylene blue on LTL-LB/HB in aqueous solution at 25 °C (inset: the structure and size of methylene blue). (D) A comparison of adsorption capacity of different zeolite L.

Note: **Supplementary Figure 11A** is exactly the same as **Figure 9B**, and it is repeated here deliberately for easier viewing and reference.

Annotation for Supplementary Figure 12 and Figure 9B:

The adsorption capacity and kinetics of methylene blue (molecular size 1.43 × 0.61 × 0.40 nm) in aqueous solution on zeolite L samples were measured as follows: 0.02 mol/L NH_4OAc aqueous solution is used as the solvent (as a buffer system with pH = 7.0) to prepare methylene blue solution with a concentration of 1.00~35.0 mg/L. For the measurement of adsorption isotherm, 20 mg of zeolite L is put into a 30 mL centrifugal tube, and 10.0 mL of the above methylene blue solutions with different concentrations is added. Subsequently, the suspension is stirred vigorously at room temperature for 12.0 h to the adsorption equilibrium. After sieving with a 0.22 μm aqueous filter, the residual concentration after adsorption is measured with a UV-Vis spectrometer at a wavelength of 661 nm to calculate the equilibrium concentration (c_e), the adsorption amount (q_e), and the adsorption efficiency at different initial concentrations (c_0).

Additionally, the measurement of adsorption kinetics is carried out at c_0 = 5 mg/L.

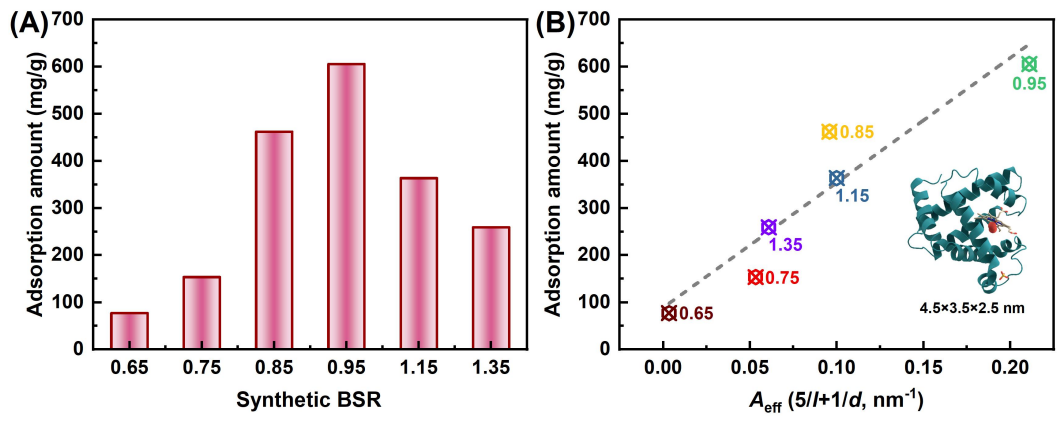

Supplementary Figure 13. (A) Comparison of myoglobin adsorption capacity of LTL mesocrystals with different morphology and size. (B) The relationship between the defined factor A_{eff} of different zeolite L with the corresponding adsorption capacity of myoglobin (inset: molecular structure and size of myoglobin).

Note: **Supplementary Figure S13B** is exactly the same as **Figure 9C**, and it is repeated here deliberately for easier viewing and reference.

Annotation for Supplementary Figure 13 and Figure 9C:

The adsorption capacity of myoglobin in aqueous solution (molecular size 4.5 × 3.5 × 2.5 nm) on zeolite L samples is measured as follows: In a commercial potassium phosphate aqueous solution buffer system (PBS, 20 mmol/L, pH = 5.0), zeolite L sample and myoglobin (both at 0.10 mg/mL) are stirred at room temperature for 1.0 h until the adsorption equilibrium. The supernatant is then separated by centrifugation at 15000 rpm for 40 min. The residual myoglobin concentration in the supernatant is measured with a UV-Vis spectrometer at a wavelength of 409 nm to calculate the adsorption amount.

In particular, based on the previous reports in the group, the adsorption capacity of the (001) crystal face for zeolite L is about 10 times that of the (100)/(010) crystal face[12]. So we may define the "effective adsorption specific area (A_{eff})" as follows:

$$\frac{10 \cdot S_{(001)} + S_{(100)/(010)}}{V} = \frac{20 \cdot \pi (d/2)^2 + \pi dl}{\pi (d/2)^2 l} = 4 \cdot \left(\frac{5}{l} + \frac{1}{d} \right). \qquad \text{(S4)}$$

For a single zeolite L particle, d is the diameter of the basal surface perpendicular to the c-axis direction, and l is the length of the c-axis; $S_{(001)}$ and $S_{(100)/(010)}$ are the basal area and lateral area exposed at the outermost side of the single L zeolite particle, respectively; V is the volume of this single L zeolite particle. Therefore, the A_{eff} can be defined as:

$$A_{eff} = \frac{5}{l} + \frac{1}{d}. \qquad \text{(S5)}$$

REFERENCES

[1] Tsapatsis M, Lovallo M, Okubo T, Davis M E, Sadakata M. Characterization of zeolite L nanoclusters. *Chem Mater*, **1995**, *7*, 1734-1741. doi: 10.1021/cm00057a025

[2] Ruiz A Z, Bruhwiler D, Ban T, Calzaferri G. Synthesis of zeolite L. Tuning size and morphology. *Monatsh Chem*, **2005**, *136*, 77-89. doi: 10.1007/s00706-004-0253-z

[3] Itani L, Bozhilov K N, Clet G, Delmotte L, Valtchev V. Factors that control zeolite L crystal size. *Chem-Eur J*, **2011**, *17*, 2199-2210. doi: 10.1002/chem.201002622

[4] Li R, Linares N, Sutjianto J G, Chawla A, Garcia-Martinez J, Rimer J D. Ultrasmall zeolite L crystals prepared from highly interdispersed alkali-silicate precursors. *Angew Chem Int Edit*, **2018**, *57*, 11283-11288. doi: 10.1002/anie.201805877

[5] Ko Y S, Ahn W S. Crystallization of zeolite L from Na_2O-K_2O-Al_2O3-SiO_2-H_2O system. *Powder Technol*, **2004**, *145*, 10-19. doi: 10.1016/j.powtec.2004.03.016

[6] Lupulescu A I, Kumar M, Rimer J D. A facile strategy to design zeolite L crystals with tunable morphology and surface architecture. *J Am Chem Soc*, **2013**, *135*, 6608-6617. doi: 10.1021/ja4015277

[7] Gomez A G, de Silveira G, Doan H, Cheng C H. A facile method to tune zeolite L crystals with low aspect ratio. *Chem Commun*, **2011**, *47*, 5876-5878. doi: 10.1039/C1CC10894H

[8] Ban T, Saito H, Naito M, Ohya Y, Takahashi Y. Synthesis of zeolite L crystals with different shapes. *J Porous Mater*, **2007**, *14*, 119-126. doi: 10.1007/s10934-006-9016-z

[9] Larlus O, Valtchev V P. Crystal morphology control of LTL-type zeolite crystals. *Chem Mater*, **2004**, *16*, 3381-3389. doi: 10.1021/cm0498741

[10] Kumar M, Li R, Rimer J D. Assembly and evolution of amorphous precursors in zeolite L crystallization. *Chem Mater*, **2016**, *28*, 1714-1727. doi: 10.1021/acs.chemmater.5b04569

[11] Groen J C, Zhu W D, Brouwer S, Huynink S J, Kapteijn F, Moulijn J A, Perez-Ramirez J. Direct demonstration of enhanced diffusion in mesoporous ZSM-5 zeolite obtained *via* controlled desilication. *J Am Chem Soc*, **2007**, *129*, 355-360. doi: 10.1021/ja065737o

[12] Hu Y Y, Zhang Y H, Ren N, Tang Y. Crystal plane- and size-dependent protein adsorption on nanozeolite. *J Phys Chem C*, **2009**, *113*, 18040-18046. doi: 10.1021/jp903989p